Phys Chem Minerals (2013) 40:341–348
DOI 10.1007/s00269-013-0575-7

ORIGINAL PAPER

Effects of pressure on $PbWO_4$-III

Dayong Tan · Wansheng Xiao · Wei Zhou · Ming Chen · Wenge Zhou · Jian Xu

Received: 1 July 2012 / Accepted: 3 February 2013 / Published online: 16 February 2013

Abstract In a hydrostatic pressure environment condition and in manual milling, respectively, investigations of $PbWO_4$-III ($P2_1/n$) have been performed by X-ray diffraction and Raman scattering techniques. Experiments found that $PbWO_4$-III keeps its monoclinic structure under hydrostatic pressures with the sample's anisotropic compressibility up to 14.6 GPa, but transforms to $PbWO_4$-I ($I4_1/a$) in a grinding process. The stability and variability of $PbWO_4$-III depending on the strain states were also explored by first-principles calculations of elasticity. Calculations show $PbWO_4$-III has an anisotropic compressibility and a ductile nature with increasing pressure up to 15 GPa.

Keywords $PbWO_4$-III · Pressure effects · Equation of state · Synchrotron X-ray diffraction · High pressure

D. Tan · W. Xiao (✉) · W. Zhou · M. Chen
Key Laboratory of Mineralogy and Metallogeny, Guangzhou Institute of Geochemistry, Chinese Academy of Sciences, Guangzhou 510640, China
e-mail: wsxiao@gig.ac.cn

D. Tan
e-mail: dytan04@gig.ac.cn

W. Zhou
Institute of Geochemistry, Chinese Academy of Sciences, Guiyang 550002, China

J. Xu
Institute of Atomic and Molecular Physics, Sichuan University, Chengdu 610065, China

J. Xu
Institute of Fluid Physics, China Academy of Engineering Physics, Mianyang 621900, China

Introduction

Lead tungstate is the most widely studied scintillating material in the family of ABO_4 compounds (A: Ca, Sr, Ba, Pb and B: W, Mo), due to its application in the detector for high-energy physics (Kobayashi et al. 1993; Lecoq et al. 1995). Under ambient conditions, there are three types of polymorphs for $PbWO_4$ compound: the tetrahedral stolzite ($PbWO_4$-I, $I4_1/a$, $Z = 4$), which has a same structure with the scheelite ($CaWO_4$), the monoclinic raspite ($PbWO_4$-II, $P2_1/a$, $Z = 4$) and the metastable monoclinic $PbWO_4$-III ($P2_1/n$, $Z = 8$) (Chipaux et al. 2001; Li et al. 2003). For their crystal structures, stolzite has isolated WO_4 tetrahedra with the Pb atom being eight-coordinated by the oxygen atoms (Chang 1971). Raspite contains edge-sharing distorted WO_6 octahedra forming continuous chains, and the Pb atom is seven-coordinated (Fujita et al. 1977). $PbWO_4$-III is built up of zigzag layers of WO_6 octahedra parallel to the a-axis, the zigzag layer consists of eight- and four-membered rings of WO_6 octahedra by edge- and corner-sharing, and the Pb atom is eight-coordinated (Richter et al. 1976). The crystal structure of $PbWO_4$-III is shown in Fig. 1.

The structural stability of stolzite ($PbWO_4$-I) has been extensively investigated by Raman spectroscopy, X-ray diffraction, X-ray absorption near-edge structure and neutron diffraction (Jayaraman et al. 1985; Christofilos et al. 2006; Manjon et al. 2006; Zhu et al. 2006; Errandonea et al. 2006a, b; Grzechnik et al. 2006). Previous investigations show that $PbWO_4$-I has a pressure-induced structural distortion from tetragonal to monoclinic symmetry following the structural sequence: scheelite ($I4_1/a$) → fergusonite ($I2/a$) → $P2_1/n$, with the different phase-transition pressures being dependent on the sensibility of different techniques (Manjon et al. 2006; Lopez-Solano et al. 2007;

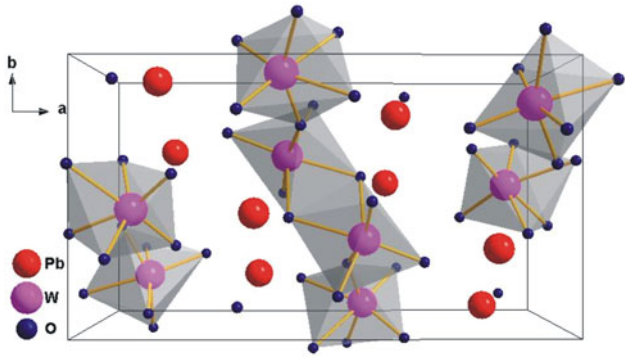

Fig. 1 (color online) Crystal structure of $PbWO_4$-III. The *zigzag layers* of WO_6 octahedra parallel to the *a*-axis and are linked by Pb atoms

Errandonea and Manjon 2008). For raspite ($PbWO_4$-II), a thermal-driven raspite to scheelite-structured transition was identified at 538 °C by an in situ transmission electron microscopy observation (Wang et al. 2011). Monoclinic $PbWO_4$-III ($P2_1/n$, $Z = 8$) structure as a high-pressure polymorph has been proposed in a large number of scheelite-type tungstates and molybdates (Fukunaga and Yamaoka 1979; Errandonea and Manjon 2008). However, a detailed high-pressure study of the X-ray diffraction and Raman scattering of $PbWO_4$-III is still lacking. In this work, we synthesized the $PbWO_4$-III using the high-pressure and high-temperature method described by the reference (Chang 1971) and investigated its structural behaviors under different strain states by the in situ Raman spectroscopy and X-ray diffraction. Furthermore, the first-principles calculations of elasticity of the $PbWO_4$-III have been carried out at various pressures up to 15 GPa.

Experimental and computational details

The sample of $PbWO_4$-III was synthesized at 4.5 GPa and 650 °C for 8 h with a cubic-anvil apparatus. Scheelite-structured $PbWO_4$-I was used as the starting material and sealed in a copper capsule. The Raman measurement on the quenched crystal product indicates that it is a pure $PbWO_4$-III phase by comparison with the Raman spectroscopy of the isomorphous $BaWO_4$-II (Tan et al. 2009). However, by simple manual grinding of the $PbWO_4$-III crystal sample using an agate pestle and mortar, a new Raman peak appears at 903 cm^{-1}. The intensity of new Raman peak increases with increase in the grinding time. The powder X-ray diffraction indicates that the additional new phase, which was produced by grinding process, belongs to the scheelite-structured $PbWO_4$-I (Chipaux et al. 2001; Richter et al. 1976). The synthesized crystal and fine grinding powder were used for our Raman and synchrotron angle-dispersive X-ray diffraction (ADXRD) measurements, respectively. The high-pressure Raman and X-ray diffraction studies were carried out by a symmetric Mao-Bell-type diamond anvil cell (DAC) with a pair of 400-μm culet diamond anvils. The T301 stainless steel gasket was pre-indented to an initial thickness of about 50 μm and then drilled a 120-μm hole serving as the sample chamber. A methanol–ethanol–water (16:3:1) mixture was used as the pressure-transmitting medium. The pressure was measured by the shift of the R1 photoluminescence line of ruby (Mao et al. 1986).

Raman spectra were recorded by a Renishaw 2000 micro-Raman spectrometer in a backscattering geometry. An argon-ion laser operating at a line of 514.5 nm was used as an exciting source. A thermoelectrically cooled CCD detector was equipped to collect the scattered light dispersed by a 1,800 lines mm^{-1} grating. All the measurements were carried out at room temperature. Reasonably good Raman data could be obtained with a collection time of about 120 s at the laser power level of 20 mW.

The ADXRD patterns were collected at the 4W2 beamline of the high-pressure station of the Beijing Synchrotron Radiation Facility (BSRF) with a monochromatic X-ray beam $\lambda = 0.6199$ Å calibrated by scanning through the Mo metal *K*-absorption edge. The X-rays were focused to a beam of 20 (vertical) × 30 (horizontal) μm^2 and the diffraction, collected on a MAR-3450 imaging plate, was converted to one-dimensional diffraction profiles using the FIT2D software (Hammersley et al. 1996). The indexing and refinement of the powder patterns were performed by using the Dicvol04 (Boultif and Louer 2004) and GSAS-EXPGUI (Toby 2001) software packages.

The accurate calculation of elasticity is essential for understanding the macroscopic mechanical properties of solids. Elasticity describes the response of a crystal under external strain and provides key information of the strength of the material, as characterized by elastic constants. The first-principles calculations were performed by using the CASTEP code (Clark et al. 2005) in the framework of density functional theory (DFT) with the local-density approximation (LDA) ultrasoft pseudopotentials and the Ceperley–Alder–Perdew–Zunger (CA-PZ) as the exchange-correlation function. The calculations employ the primitive cell of $PbWO_4$-III, containing 48 atoms. Geometry optimization is conducted using convergence thresholds of 1.0×10^{-5} eV $atom^{-1}$ for the total energy, 0.03 eV $Å^{-1}$ for maximum force, 0.05 GPa for maximum stress and 1.0×10^{-3} Å for maximum displacement. A 530.0 eV plane-wave energy cutoff and $1\times2\times2$ Monkhorst–Pack grids (Monkhorst and Pack 1976) for the Brillouin zone sampling were used in all the elastic properties calculations for $PbWO_4$-III. The pressure is increased from zero pressure to 15 GPa in an increment of 2.5 GPa.

Results and discussions

Raman scattering

The Raman spectra of $PbWO_4$-III at several representative pressures are shown in Fig. 2. Table 1 exhibits the observed frequencies of various Raman modes at the room pressure (0.1 MPa) and their pressure coefficients. Series of the Raman spectra show a very similar profile. With increasing pressure, the observed Raman peaks shift continuously toward higher wavenumbers and no additional Raman peak appears. This feature indicates that the $PbWO_4$-III is stable at least up to 14.6 GPa under hydrostatic conditions at room temperature. For the room pressure Raman spectra, 31 Raman bands are observed in a wavenumber range of 100–1,000 cm^{-1}, which are more than 13 and 18 Raman-active modes of the tetrahedral stolzite ($PbWO_4$-I, $I4_1/a$) and the monoclinic raspite ($PbWO_4$-II, $P2_1/a$) (Bastians et al. 2004), respectively, but less than 72 Raman-active modes of the $PbWO_4$-III ($P2_1/n$) structure expected by the group theory analysis ($\Gamma_{\text{Raman}} = 36A_g + 36B_g$) (Manjon et al. 2006; Rousseau et al. 1981). Another feature of Raman spectra shows that the most intense vibration is not the highest frequency vibration (the most intense mode at 870.5 cm^{-1} and the highest frequency mode at 916.6 cm^{-1}), which is similar to the Raman spectra of isomorphous $BaWO_4$-II ($P2_1/n$) (Tan et al. 2009), but is different from the Raman spectra of raspite ($PbWO_4$-II) and stolzite ($PbWO_4$-I) (Bastians et al. 2004). The existence of only a single sharp and intense Raman peak of $PbWO_4$-III also shows the difference from a couple of intense peaks at 899 and 914 cm^{-1} at 13.7 GPa in previously observed Raman spectrum of the phase interpreted as the $PbWO_4$-III (Manjon et al. 2006).

Previous knowledge in tungstates indicates that the observed highest Raman frequency reflects the stretching modes of the WO_4 tetrahedra or the WO_6 octahedra unit in the structure, the frequencies ω (cm^{-1}) of the stretching W–O modes have a direct relationship to the bond distance R (in Å) between W and O in tungsten oxides, ω (cm^{-1}) = 25,823 exp (−1.902 R) (Hardcastle and Wachs 1995). In $PbWO_4$-III, the average W–O bond distance of WO_6 octahedra (1.96 Å) (Richter et al. 1976) is close to the 1.94 Å in raspite and remarkably longer than the 1.795 Å in the stolzite. Therefore, the frequency of WO_6 octahedra stretching mode in $PbWO_4$-III is near raspite's 870 cm^{-1} but not stolzite's 910 cm^{-1} (Bastians et al. 2004). This can be rationalized on the simplistic basis that the intense 870.5 cm^{-1} mode in $PbWO_4$-III represents stretching mode of the WO_6 octahedra. Further, based on the ab initio lattice dynamics calculations in isomorphous phase of $BaWO_4$-II, the similar most intense Raman peak might be assigned to the A_g mode (Lacomba-Perales et al. 2010).

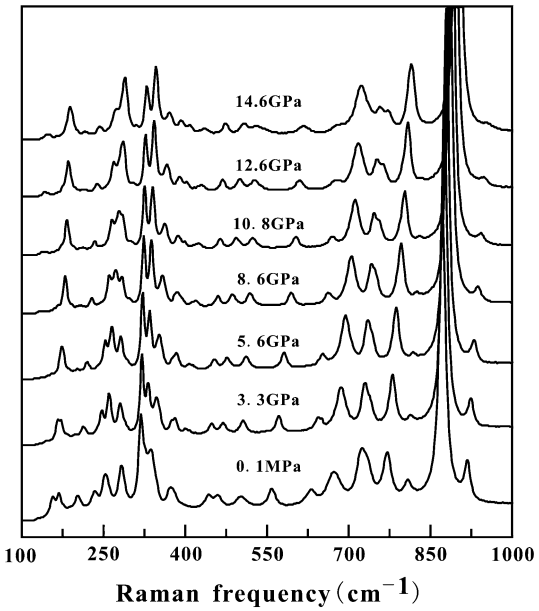

Fig. 2 Representative Raman spectra of $PbWO_4$-III under ambient and high pressures at room temperature

Figure 3 shows the representative Raman spectra obtained from the $PbWO_4$-III sample by simple manual grinding using an agate mortar and pestle. These spectra display three primary characters. Firstly, with increasing milling time, new Raman peaks appear sequentially at 903, 754 and 358 cm^{-1}. Secondly, the new Raman peaks progressively obtain intensity with increase in the milling time. On the contrary, the peaks related to $PbWO_4$-III phase progressively become weaker and weaker. Finally, the new Raman peaks after milling about 25 min are very accordant with that of the stolzite ($PbWO_4$-I). These characters indicate that the $PbWO_4$-III transforms to the $PbWO_4$-I by the grinding process.

X-ray diffraction

Owing to the severe peaks overlapping in the high-angle region and the uneven distribution of peak intensities in the diffraction rings of the monoclinic $PbWO_4$-III, we show the ADXRD patterns only at angles 5°–15° and further weaken the most intense lines (about 11°–12°) to half its original intensities. The selected ADXRD patterns of the powder sample at several pressures are shown in Fig. 4. The existence of two intense diffraction lines located near 11°–12° shows distinct difference from one intense broad peak of the proposed $PbWO_4$-III by Errandonea et al. (2006b). Compared with the crystal diffraction data of $PbWO_4$-III and $PbWO_4$-I (Richter et al. 1976; Chipaux et al. 2001), our powder ADXRD patterns indicate that the grinding powder sample includes two phases. The calculated positions of the diffraction peaks of the tetrahedral

Table 1 Observed Raman modes of $PbWO_4$-III at 0.1 MPa and their pressure derivatives ($d\omega/dP$)

Peak	ω (0) (cm^{-1})	$d\omega/dP$ (cm^{-1}/GPa)	Peak	ω (0) (cm^{-1})	$d\omega/dP$ (cm^{-1}/GPa)
1	916.6	2.31 (4)	17	376.7	2.18 (7)
2	870.5	1.93 (6)	18	371.5	1.53 (5)
3	807.6	2.10 (3)	19	338.7	2.14 (3)
4	770	3.03 (2)	20	328.5	1.21 (2)
5	733.3	1.50 (4)	21	318.9	0.73 (3)
6	722.6	2.32 (4)	22	283.9	1.74 (7)
7	715.8	3.70 (9)	23	281.1	0.52 (3)
8	673	3.46 (5)	24	253.6	2.44 (5)
9	631.3	3.56 (4)	25	235.8	2.61 (8)
10	558.5	4.11 (4)	26	204.9	2.78 (4)
11	501.4	2.22 (5)	27	193.6	1.74 (5)
12	458.8	3.30 (2)	28	177	1.86 (8)
13	443.6	2.08 (4)	29	168.7	1.46 (3)
14	390.9	2.67 (7)	30	157.3	2.63 (9)
15	389.9	3.28 (9)	31	138.8	3.22 (8)
16	378.9	0.96 (2)			

Here, $d\omega/dP$ is obtained through a linear fitting of ω–P data between 0 and 14.6 GPa

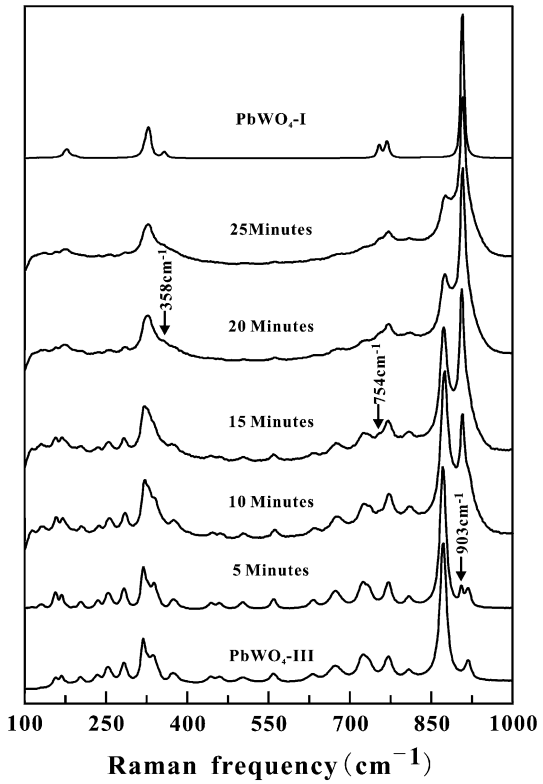

Fig. 3 The Raman spectra of $PbWO_4$-I and $PbWO_4$-III with different milling times

$PbWO_4$-I and the monoclinic $PbWO_4$-III are indicated by arrows and tick marks in Fig. 4, respectively. According to the Raman investigations, the fewer $PbWO_4$-I phase was caused by grinding from the synthesized $PbWO_4$-III. As shown in Fig. 4, the observed diffraction peaks of $PbWO_4$-III shift smoothly with pressures up to the highest experimental pressure 13.4 GPa. But the diffraction peaks of $PbWO_4$-I have an obvious change at the pressure increasing up to 7.0 GPa. The value of the phase-transition pressure is in good agreement with that reported previously in the phase transition of the scheelite-type $PbWO_4$-I (Errandonea et al. 2006b).

From the diffraction patterns collected at different pressures, we extracted the pressure evolution of the unit-cell parameters of $PbWO_4$-III up to 13.4 GPa. Results are summarized in Table 2 and Figs. 5, 6. In Figs. 5 and 6, the lattice parameters normalized by the ambient pressure are plotted as a function of pressure. The smooth curves in this graph reveal that there is no phase transition in the pressure range of our experiments. The pressure–volume data have been fitted to a third-order Birch–Murnaghan equation of state

$$P = \frac{3}{2}K_0\left[\left(\frac{V_0}{V}\right)^{7/3} - \left(\frac{V_0}{V}\right)^{5/3}\right] \times \left\{1 + \frac{3}{4}(K' - 4)\left[\left(\frac{V_0}{V}\right)^{2/3} - 1\right]\right\},$$

where P, V_0, K_0 and K' are the pressure, zero-pressure volume, isothermal bulk modulus and the pressure derivative of isothermal bulk modulus, respectively (Birch 1947). Our results with the data collected below 13.4 GPa suggest that K_0 = 87.4 ± 2.4 GPa, with a fixed unit-cell volume V_0 = 659.00 $Å^3$ and a pressure derivative K' = 4. Since the data collected at pressures above 10 GPa were potentially affected by the inhomogeneous stress in a diamond cell due to the solidification of the pressure media at about 10 GPa (Klotz et al. 2009), we also tried our calculation with the data gathered at the pressure below 10 GPa. A least-square fitting using the third-order Birch–Murnaghan equation of state yields an isothermal bulk modulus of K_0 = 79.2 ± 0.9 GPa with V_0 = 659.00 $Å^3$ and K' = 4. It is similar with the bulk modulus (K_0 = 76.7 ± 0.7 GPa) of the same structural phase $BaWO_4$-II (Tan et al. 2012) and is larger than the bulk modulus (K_0 = 66 ± 5 GPa) of the scheelite-type $PbWO_4$-I (Errandonea et al. 2006b). According to Xu et al. (1994), the linear bulk modulus in the a-axis (K_0 (a) = 191.7 ± 1.9 GPa) is only about 76 % of that in the b-axis (K_0 (b) = 251.2 ± 2.3 GPa) and 55 % of that in the c-axis (K_0 (c) = 348.9 ± 2.5 GPa). As a result, the compressibility of a-axis is much larger than the b-axis or c-axis.

We have also refined the diffraction pattern of $PbWO_4$-III phase at 13.4 GPa. The starting atomic parameters for the refinement in the structure model were taken from single-crystal diffraction experiment (Richter et al. 1976).

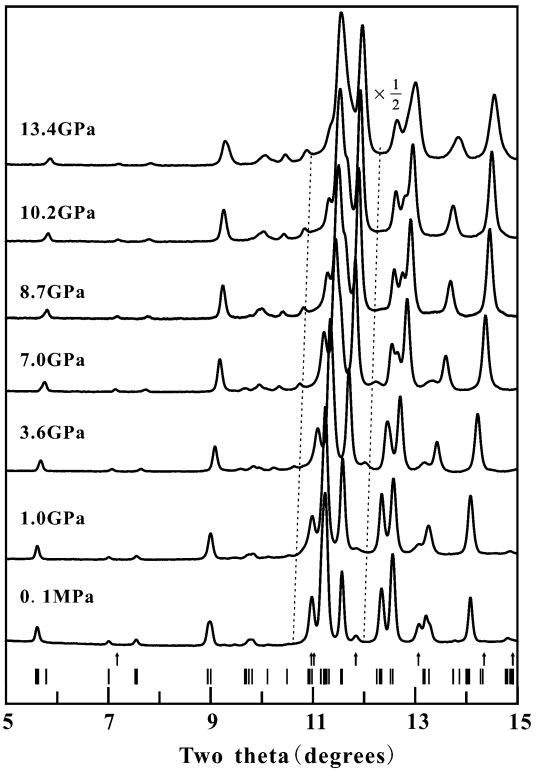

Fig. 4 Representative X-diffraction spectra of the $PbWO_4$-III at several pressures. *Tick marks* represent the calculated positions of the diffraction peaks of the monoclinic $PbWO_4$-III structure. The reflections of the tetrahedral $PbWO_4$-I are indicated by *arrows*

Table 2 Lattice parameters collected at different pressures for $PbWO_4$-III

P (GPa)	*a* (Å)	*b* (Å)	*c* (Å)	Beta (°)	*V* (Å^3)
0.0001	12.725 (5)	7.051 (4)	7.345 (4)	90.35 (5)	659.0 (4)
0.6	12.677 (4)	7.027 (3)	7.330 (4)	90.27 (4)	652.9 (3)
1.04	12.657 (4)	7.016 (3)	7.319 (4)	90.22 (4)	649.9 (3)
1.84	12.603 (6)	6.989 (5)	7.296 (5)	90.13 (6)	642.6 (4)
3.61	12.509 (6)	6.947 (5)	7.258 (5)	90.05 (6)	630.7 (4)
4.99	12.430 (7)	6.911 (6)	7.230 (7)	89.91 (8)	621.1 (5)
7.04	12.342 (6)	6.872 (5)	7.203 (6)	89.86 (7)	610.9 (5)
8.74	12.216 (2)	6.834 (1)	7.176 (1)	89.68 (1)	599.1 (2)
10.2	12.197 (7)	6.818 (5)	7.158 (5)	89.66 (8)	595.3 (5)
11.66	12.174 (7)	6.807 (6)	7.156 (7)	89.63 (9)	593.0 (5)
12.59	12.147 (8)	6.800 (6)	7.154 (7)	89.52 (9)	590.6 (6)
13.37	12.082 (2)	6.792 (1)	7.153 (1)	89.43 (1)	587.0 (2)

The refinement parameters included the scale factor and 20 background terms in a shifted Chebyschev polynomial function. Peak profiles were modeled using a pseudoVoigt profile function with GU, GV, GW, asymmetry corrections and anisotropic broadening terms. After convergence of these parameters, the unit-cell dimensions, final atomic coordinates and isotropic thermal parameters were

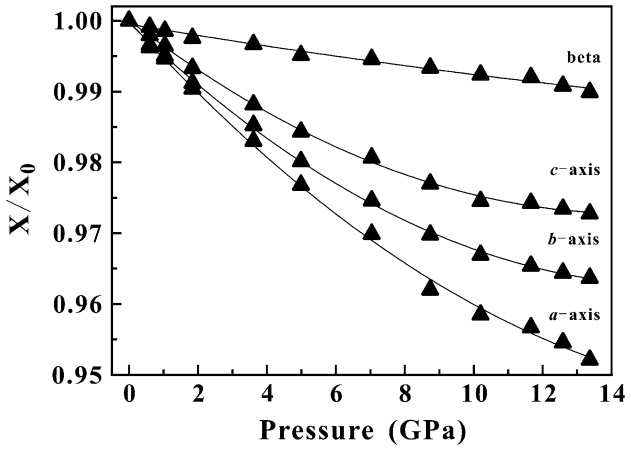

Fig. 5 Unit-cell parameters of $PbWO_4$-III phase as a function of pressure. Data normalized with respect to the room-pressure values. The *solid line* is the polynomial fitting to data points

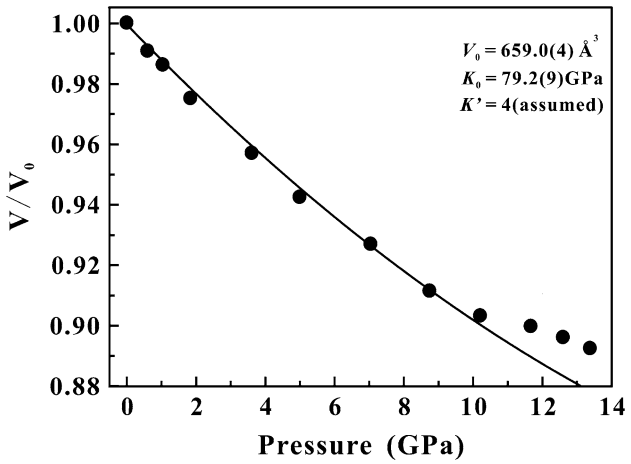

Fig. 6 Pressure dependence of relative volume (V/V_0) for $PbWO_4$-III phase. The *solid line* presents a third-order Birch–Murnaghan equation of state fitting to the gathered experimental data at pressure below 10 GPa

successively refined. Owing to the small X-ray scattering cross-section of the oxygen atoms comparing to the tungsten and lead atoms, it is difficult to determine accurately the 24 oxygen atom coordinates by the present powder X-ray diffraction pattern. Therefore, during the refinement of the atomic coordinates, the oxygen atom coordinates were constrained to the original positions (Richter et al. 1976). Only the Pb and W positions were refined. The refinement results are given in Table 3 and Fig. 7. The small residuals and the good match of the calculated and observed diffraction patterns indicate that the monoclinic $PbWO_4$-III structural model can fit the experimental data very well. Therefore, we think that the $PbWO_4$-III polymorph keeps its zero-pressure monoclinic structure under pressure up to 13.4 GPa.

Table 3 Refined structural parameters of $PbWO_4$-III phase at 13.4 GPa

Atom	Site	*x*	*y*	*z*
Pb_1	4*e*	0.1610 (08)	0.6804 (16)	0.1704 (15)
Pb_2	4*e*	0.1314 (09)	0.9607 (13)	0.6279 (20)
W_1	4*e*	0.0894 (12)	0.1681 (21)	0.0808 (17)
W_2	4*e*	0.0994 (10)	0.4706 (14)	0.6399 (18)

$a = 12.0822$ (22) Å, $b = 6.7920$ (5) Å, $c = 7.1531$ (8) Å, $\beta = 89.43$ (1)°. $R_{wp} = 4.9$ %, $R_p = 3.7$ %, $R(F^2) = 8.6$ %

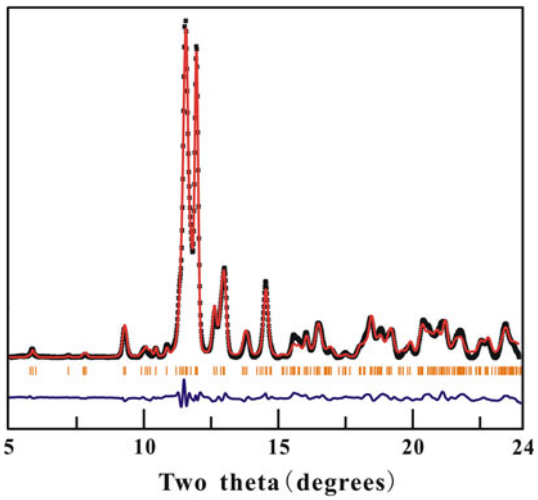

Fig. 7 (color online) Final Rietveld fits for the $PbWO_4$-III phase at 13.4 GPa. The experimentally observed data are indicated by *crosses* (*black*), the calculated pattern is the *continuous line* (*red*) and the *lower curve* (*blue*) is the weighted difference between the calculated and observed patterns. Background was subtracted. *Tick marks* represent the calculated positions of the diffraction peaks of the $PbWO_4$-III structure (*orange*)

Elastic properties

We adopt the stress–strain method to evaluate the full elastic constants of $PbWO_4$-III. In the method, the stain–stress curve is described by the well-known relationship, the Hooker's law,

$$\sigma_{ij} = C_{ijkl}\varepsilon_{kl}\,(i,j,k,l = 1,2,3)$$

where σ_{ij} is the stress tensor, ε_{kl} is the Lagrangian strain tensor and C_{ijkl} is the elastic constant tensor which is a 6×6 matrix (36 elements in general cases). For a monoclinic crystal, the independent elastic constant tensor reduces to 13 components of C_{11}, C_{22}, C_{33}, C_{44}, C_{55}, C_{66}, C_{12}, C_{13}, C_{23}, C_{15}, C_{25}, C_{35} and C_{46}. The elastic constants (C_{ijkl}) of $PbWO_4$-III calculated by using the CASTEP code are listed in Table 4. The calculated results show that the six elastic constants $C_{ijkl}^{ij=kl}$ are positive ($C_{11} > 0$, $C_{22} > 0$, $C_{33} > 0$, $C_{44} > 0$, $C_{55} > 0$ and $C_{66} > 0$). Since the values of the $C_{ijkl}^{ij=kl}$ are larger than that of the C_{12}, C_{13}, C_{15}, C_{23}, C_{25}, C_{35} and C_{46}, the relation of $C_{ijij}C_{klkl} > C_{ijkl}^2$ (e.g., $C_{33}C_{55} > C_{35}^2$) can be deduced. A further analysis indicates that all the values of elastic constants satisfy the mechanical stability criteria for monoclinic system (Nye 1985; Wu et al. 2007), which suggests that $PbWO_4$-III is mechanically stable in the pressure range of 0–15 GPa.

Figure 8 displays the pressure evolution of the elastic constants C_{ijkl}. We found that the elastic constants C_{ijkl} have a monotonous variation with increasing pressure, and their magnitudes are quite different. With increasing pressures up to 15 GPa, the C_{11}, C_{22}, and C_{33} values increase significantly, whereas C_{44}, C_{55} and C_{66} change a little and are almost constant in this pressure range.

Table 4 Calculated values for elastic stiffness coefficients (C_{ijkl} in GPa), bulk modulus (*K* in GPa), shear modulus (*G* in GPa) and the ratio *K*/*G* of $PbWO_4$-III

P = 0 (GPa)		2.5 (GPa)	5 (GPa)	7.5 (GPa)	10 (GPa)	12.5 (GPa)	15 (GPa)
C_{11}	119.79	145.75	165.09	176.51	193.54	208.62	224.55
C_{22}	140.98	187.68	198	234.61	263.36	289.61	295.36
C_{33}	166.11	179.52	207.24	233.25	256.86	288.95	296.03
C_{44}	46.47	54.09	53.33	65.11	68.57	68.3	65.08
C_{55}	46.82	47.63	53.77	62.26	66.09	75.76	75.05
C_{66}	38.68	44.24	52.84	52.43	57.37	62.8	62.89
C_{12}	43.85	65.75	75.78	97.76	110.27	118.41	124.11
C_{13}	75.67	80.42	94.11	108.22	124.52	131.64	137.69
C_{15}	12.03	11.52	11.66	7.62	6.43	8.24	7.4
C_{23}	62.23	73.63	87.33	108.81	125.28	139.49	143.38
C_{25}	5.75	8.61	6.56	1.82	2.57	4.63	6.65
C_{35}	−0.44	9.08	7.9	6.06	7.19	1.54	4.45
C_{46}	1.56	−0.8	−2.38	−5.76	−7.34	−7.61	−6.52
K	85.24	104.11	118.89	139.68	157	167.62	178.21
G	41.76	48.17	52.46	57.14	61.07	66.01	67.29
K/*G*	2.04	2.16	2.27	2.44	2.57	2.54	2.65

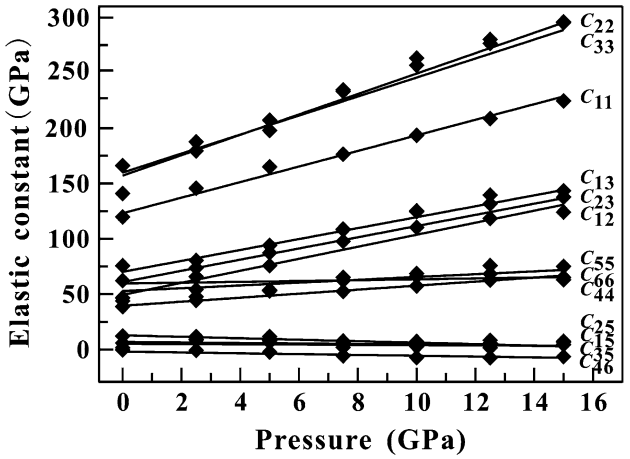

Fig. 8 Pressure evolutions of the elastic stiffness coefficients of $PbWO_4$-III phase

In particular, it is noteworthy that C_{15}, C_{25}, C_{35} and C_{46} values are close to zero. These behaviors of the elastic constants show an elastic anisotropy of the $PbWO_4$-III. Using the calculated elastic constants C_{ijkl}, bulk modulus and shear modulus for the corresponding polycrystalline aggregate can be determined by the Voig–Reuss–Hill approximation method (Hill 1952). The bulk modulus K and the shear modulus G are also listed in Table 4. Clearly, the calculated bulk modulus $K = 85.2$ GPa under the ambient pressure agrees well with our experimental data $K_0 = 79.2$ GPa, supporting the accuracy and reliability of our elastic calculations. In order to further insight the stability and variability of $PbWO_4$-III, we consider the Pugh's criteria: a material behaves in a ductile manner if $K/G > 1.75$, otherwise it should be brittle (Pugh 1954). With increasing pressure, the K/G ratios of $PbWO_4$-III increase from 2.04 to 2.65. These K/G ratios are all greater than the "critical" value of ~ 1.75, indicating the ductile nature of $PbWO_4$-III.

Conclusions

A pure $PbWO_4$-III phase has been synthesized at 4.5 GPa and 650 °C with a cubic-anvil apparatus, and the effects of pressures on $PbWO_4$-III were investigated. The X-ray diffraction and Raman experiments show that $PbWO_4$-III remains its monoclinic structure with an anisotropic compressibility under pressure up to 14.6 GPa, but changes to $PbWO_4$-I ($I4_1/a$) by grinding process. The calculated elastic constants and the K/G ratios show that $PbWO_4$-III has an anisotropic compressibility and a ductile nature with increasing pressure up to 15 GPa.

Acknowledgments We thank Editor Prof. Matsui and two anonymous reviewers for the constructive comments and suggestions. We gratefully acknowledge the help from High-pressure Beam Line, BSRF, China. The work has been supported by the National Natural Science Foundation of China (41272058, 11179030 and 10874158), GIGCAS 135 project Y234101001 and the Foundation of China Academy of Engineering Physics under Grant No. 2008A0101001.

References

Bastians S, Crump G, Griffith WP, Withnall R (2004) Raspite and studtite: Raman spectra of two unique minerals. J Raman Spectrosc 35:726–731

Birch F (1947) Finite elastic strain of cubic crystals. Phys Rev 71:809–824

Boultif A, Louer D (2004) Powder pattern indexing with the dichotomy method. J Appl Crystallogr 37:724–731

Chang LLY (1971) Phase relations in the system PbO–WO_3. J Am Ceram Soc 54:357–358

Chipaux R, Andre G, Cousson A (2001) Crystal structure of lead tungstate at 1.4 and 300 K. J Alloy Comp 325:91–94

Christofilos D, Efthimiopoulos E, Arvanitidis J, Papagelis K, Ves S, Kourouklis GA (2006) Raman study of polycrystalline $PbWO_4$ under high pressure. High Pressure Res 26:421–425

Clark SJ, Segall MD, Pickard CJ, Hasnip PJ, Probert MJ, Refson K, Payne MC (2005) First principles methods using CASTEP. Z Kristallogra 220:567–570

Errandonea D, Manjon FJ (2008) Pressure effects on the structural and electronic properties of ABX4 scintillating crystals. Prog Mater Sci 53:711–773

Errandonea D, Martinez-Garcia D, Lacomba-Perales R, Ruiz-Fuertes J, Segura A (2006a) Effects of high pressure on the optical absorption spectrum of scintillating $PbWO_4$ crystals. Appl Phys Lett 89:091913

Errandonea D, Pellicer-Porres J, Manjon FJ, Segura A, Ferrer-Roca C, Kumar RS, Tschauner O, Lopez-Solano J, Rodriguez-Hernandez P, Radescu S, Mujica A, Munoz A, Aquilanti G (2006b) Determination of the high-pressure crystal structure of $BaWO_4$ and $PbWO_4$. Phys Rev B 73:224103

Fujita T, Kawada I, Kato K (1977) Raspite from broken hill. Acta Crystallogr B 33:162–164

Fukunaga O, Yamaoka S (1979) Phase-transformations in ABO_4 type compounds under high-pressure. Phys Chem Miner 5:167–177

Grzechnik A, Crichton WA, Marshall WG, Friese K (2006) High-pressure X-ray and neutron powder diffraction study of $PbWO_4$ and $BaWO_4$ scheelites. J Phys: Condens Matter 18:3017–3029

Hammersley AP, Svensson SO, Hanfland M, Fitch AN, Hausermann D (1996) Two-dimensional detector software: from real detector to idealised image or two-theta scan. High Pressure Res 14:235–248

Hardcastle FD, Wachs IE (1995) Determination of the molecular structures of tungstates by Raman spectroscopy. J Raman Spectrosc 26:397–405

Hill R (1952) On discontinuous plastic states, with special reference to localized necking in thin sheets. J Mech Phys Solids 1:19–30

Jayaraman A, Batlogg B, Vanuitert LG (1985) Effect of high-pressure on the Raman and electronic absorption-spectra of $PbMoO_4$ and $PbWO_4$. Phys Rev B 31:5423–5427

Klotz S, Chervin JC, Munsch P, Le Marchand G (2009) Hydrostatic limits of 11 pressure transmitting media. J Phys D Appl Phys 42:075413

Kobayashi M, Ishii M, Usuki Y, Yahagi H (1993) Scintillation characteristics of $PbWO_4$ single-crystals at room-temperature. Nucl Instrum Method Phys Res A 333:429–433

Lacomba-Perales R, Martinez-Garcia D, Errandonea D, Le Godec Y, Philippe J, Le Marchand G, Chervin JC, Polian A, Munoz A,

Lopez-Solano J (2010) Experimental and theoretical investigation of the stability of the monoclinic $BaWO_4$-II phase at high pressure and high temperature. Phys Rev B 81:144117

Lecoq P, Dafinei I, Auffray E, Schneegans M, Korzhik MV, Missevitch OV, Pavlenko VB, Fedorov AA, Annenkov AN, Kostylev VL, Ligun VD (1995) Lead tungstate ($PbWO_4$) Scintillators for LHC EM calorimetry. Nucl Instrum Method Phys Res A 365:291–298

Li S, Ahuja R, Wang Y, Johansson B (2003) Crystallographic structures of $PbWO_4$. High Pressure Res 23:343–347

Lopez-Solano J, Rodriguez-Hernandez P, Radescu S, Mujica A, Munoz A, Errandonea D, Manjon FJ, Pellicer-Porres J, Garro N, Segura A, Ferrer-Roca C, Kumar RS, Tschauner O, Aquilanti G (2007) Crystal stability and pressure-induced phase transitions in scheelite AWO_4 (A = Ca, Sr, Ba, Pb, Eu) binary oxides. I: a review of recent ab initio calculations, ADXRD, XANES, and Raman studies. Phys Status Solidi B 244:325–330

Manjon FJ, Errandonea D, Garro N, Pellicer-Porres J, Lopez-Solano J, Rodriguez-Hernandez P, Radescu S, Mujica A, Munoz A (2006) Lattice dynamics study of scheelite tungstates under high pressure II. $PbWO_4$. Phys Rev B 74:144112

Mao HK, Xu J, Bell PM (1986) Calibration of the ruby pressure gauge to 800-k bar under quasi-hydrostatic conditions. J Geophys Res 91:4673–4676

Monkhorst HJ, Pack JD (1976) Special points for Brillouin-zone integrations. Phys Rev B 13:5188–5192

Nye JF (1985) Physical properties of crystals: their representation by tensors and matrices. Oxford University Press, Oxford

Pugh SF (1954) Relation between the elastic moduli and the plastic properties of polycrystalline pure metals. Philos Mag 45:823–843

Richter PW, Kruger GJ, Pistorius C (1976) $PbWO_4$-III (A high-pressure form). Acta Crystallogr B 32:928–929

Rousseau DL, Bauman RP, Porto SPS (1981) Normal mode determination in crystals. J Raman Spectrosc 10:253–290

Tan DY, Xiao WS, Zhou WG, Song MS, Xiong XL, Chen M (2009) Raman Investigation of $BaWO_4$-II phase under hydrostatic pressures up to 14.8 GPa. Chin Phys Lett 26:046301

Tan D, Xiao W, Zhou W, Chen M, Zhou W, Li X, Li Y, Liu J (2012) High pressure X-ray diffraction study on $BaWO_4$-II. High Pressure Res 32:262–269

Toby BH (2001) EXPGUI, a graphical user interface for GSAS. J Appl Crystallogr 34:210–213

Wang X, Ding Y, Wang ZL, Hu C (2011) Temperature driven in-situ phase transformation of $PbWO_4$ nanobelts. J Appl Phys 109:124309

Wu Z-j, Zhao E-j, Xiang H-p, Hao X-f, Liu X-j, Meng J (2007) Crystal structures and elastic properties of superhard IrN2 and IrN3 from first principles. Phys Rev B 76:054115

Xu JA, Hu JZ, Ming LC, Huang E, Xie HS (1994) The compression of diaspore, AlO(OH) at room-temperature up to 27 GPa. Geophys Res Lett 21:161–164

Zhu WL, Wan KS, Huang YL, Feng XQ, Pezzotti G (2006) Stress dependence of Raman vibrational bands of $PbWO_4$ single crystals. Phys Status Solidi A 203:2376–2385